Quantum Electronics **48** (8) 728–732 (2018)

FIBRE OPTICS

https://doi.org/10.1070/QEL16695

Narrow-band fibre reflector based on a fibre Bragg grating reflection interferometer

V.S. Terentyev, A.A. Vlasov, S.R. Abdullina, V.A. Simonov,
M.I. Skvortsov, S.A. Babin

Abstract. **Narrow-band filtering in reflected light using a reflection interferometer with a fibre Bragg grating (FBG) as its back mirror is demonstrated for the first time. The reflection interferometer is made in SMF-28e single-mode fibre, and the faces of its front mirror, which includes a thin metallic film, differ in reflectance. The reflection bandwidth of a test sample is 0.5 pm (62 MHz) at a wavelength of 1556 nm (Q-factor of 3×10^6), its maximum reflectance is 0.21, and its contrast is 10^2. The use of a narrow-band FBG instead of thin-film broadband mirrors allows spectral selection to be significantly improved owing to an increase in the length of the interferometer base.**

Keywords: *fibre optics, multiple-beam interference, reflection interferometer, thin metallic film, dielectric interference coating, fibre Bragg grating.*

1. Introduction

Narrow-band all-fibre spectral filters are used in spectroscopy, for laser wavelength selection and in sensor systems. There are a variety of light filtering methods, the most widespread of which are transmission filtering methods, where light passes through a filter (Fabry–Perot interferometer [1], distributed feedback cavity [2], ring cavities, whispering gallery mode cavities [3, 4] and others). These methods are inapplicable to problems that require narrow-band reflection filtering (e. g. single-frequency spectral selection for waveguide lasers or linear-cavity laser diodes). Possible reflection filters include fibre Bragg gratings (FBGs), in particular, argon laser-inscribed long FBGs [5] and ultralong FBGs produced by a femtosecond laser modification method [6], as well as fibre and integrated optic multiple cavity systems [7]. The above methods have certain drawbacks, e.g. a comparatively broad spectral band of selection (above 100 pm for ordinary FBGs) or relatively complex technology and increased sensitivity of parameters of filters to vibrations and temperature fluctuations because of the long length of their silica cavities. For single-frequency laser output selection purposes, it is desirable to have a reflection filter with a spectrally narrow reflection peak throughout the gain range of the active medium. The peak can be nonunique, but its height should considerably exceed that of the other peaks, which is of particular importance for media with a wide spectral gain range, e. g. for those based on Er^{3+} and Yb^{3+} ions or semiconductor optical amplifiers. The use of a fibre reflection interferometer with broadband dielectric mirrors for single mode selection [8] indicates that multiple spectral orders of interference in reflection may play a parasitic role, in particular, reducing the signal-to-noise ratio, and potentially create conditions for multiwavelength lasing.

The purpose of this work is to demonstrate a method for producing a spectrally narrow reflection peak for narrow-band light filtering or intracavity single-frequency selection of fibre or waveguide cavity laser light using a reflection interferometer [9] based on a metal-coated mirror and FBG. The distinctive features of this method are the use of a fibre cavity – similar to a Fabry–Perot cavity – formed by an asymmetric thin-film mirror and an FBG written by UV laser radiation through a phase mask. It offers the advantages of relative simplicity and technological feasibility, ensuring a rather high quality factor (above 10^6) of the reflection filter, whose dimensions ($\varnothing 3\times 50$ mm) facilitate temperature and vibration stabilisation of its parameters.

2. FBG reflection interferometer

Figure 1a shows a schematic of a filter in the form of an FBG-based reflection interferometer. It consists of two single-mode optical fibres placed in fibre ferrules up to 15 mm in length (with a metallic flange), centred using a cylindrical spring of 3.2 mm outer diameter. The end facet of the left-hand optical fibre (OF) has a mirror whose faces differ in reflectance [asymmetric mirror (AM) in what follows] and which comprises a thin metallic film and dielectric interference coating. The asymmetric mirror can have very low reflectance on the light source side and high reflectance on the opposite side: $0 \leftarrow R_1 \ll R_2 < 1$ (R_2 can approach unity). This strong asymmetry is due to the presence of a thin metallic (nickel) film of thickness $h \approx 10$ nm, which produces a considerable loss ($\sim$30%) for a travelling light wave as a result of Ohmic absorption. In the case of a standing wave, the loss due to such a film will depend on its position: at a standing wave node, where the field has the minimum amplitude, the loss in the film decreases substantially [by a factor of $\sim(\lambda/h)^2$, where λ is the wavelength in vacuum]. The properties of an optimised structure of the asymmetric mirror ($R_1 \to 0$) are such that the optical thicknesses of the layers in the dielectric interference coating should not be a multiple of a quarter wavelength, with the

V.S. Terentyev, A.A. Vlasov, S.R. Abdullina, V.A. Simonov Institute of Automation and Electrometry, Siberian Branch, Russian Academy of Sciences, prosp. Akad. Koptyuga 1, 630090 Novosibirsk, Russia; e-mail: terentyev@iae.nsk.su;
M.I. Skvortsov, S.A. Babin Institute of Automation and Electrometry, Siberian Branch, Russian Academy of Sciences, prosp. Akad. Koptyuga 1, 630090 Novosibirsk, Russia; Novosibirsk State University, ul. Pirogova 1, 630090 Novosibirsk, Russia

Received 9 April 2018; revision received 16 May 2018
Kvantovaya Elektronika **48** (8) 728–732 (2018)
Translated by O.M. Tsarev

thickness of the first layer differing little from it, whereas the thicknesses of the other layers can differ from it by up to 10% [10]. The scattering (diffraction divergence) loss during the propagation of the fundamental mode of the fibre across the AM can be neglected because the geometric thickness of the mirror for about ten TiO_2 and SiO_2 dielectric layers is negligible ($L_{am} < 1.5\lambda$). The transmission of the asymmetric mirror is reciprocal ($T_1 \equiv T_2$), with $T_1 \to (1 - R_2)/2$ for $R_1 \to 0$ [10]. The right-hand fibre has an FBG with reflectance R_3 a distance L_{fib} from its end facet (reflection from the facet–air interface is left out of account). In the plane wave approximation, the amplitude reflection (r) and transmission (t) coefficients of such an interferometer have the form [11]

$$r = r_1 + \frac{t_1 t_2 r_3 \exp(-i2\psi)}{1 - r_2 r_3 \exp(-i2\psi)}, \quad (1)$$

$$t = \frac{t_1 t_3 \exp(-i\psi)}{1 - r_2 r_3 \exp(-i2\psi)}, \quad (2)$$

where the amplitude coefficients of the mirrors, $r_j = \sqrt{R_j} \times \exp(i\Psi_j)$ and $t_j = \sqrt{T_j}\exp(i\Phi_j)$ ($j =$ 1 and 2 for the two sides of the AM and $j = 3$ for the FBG), are expressed through the power reflection (R_j) and transmission (T_j) coefficients and their phases Ψ_j and Φ_j; $\psi = 2\pi L/\lambda$; $L = L_{fs} + n(L_{fib} + L_{eff})$ is the total optical length of the interferometer base; L_{fs} is the length of the air gap; L_{fib} is the length of the fibre section in front of the FBG; L_{eff} is the effective FBG length [12]; n is the effective refractive index of the fundamental mode of the fibre portion of the interferometer base; $R = |r|^2$; and $T = |t|^2$.

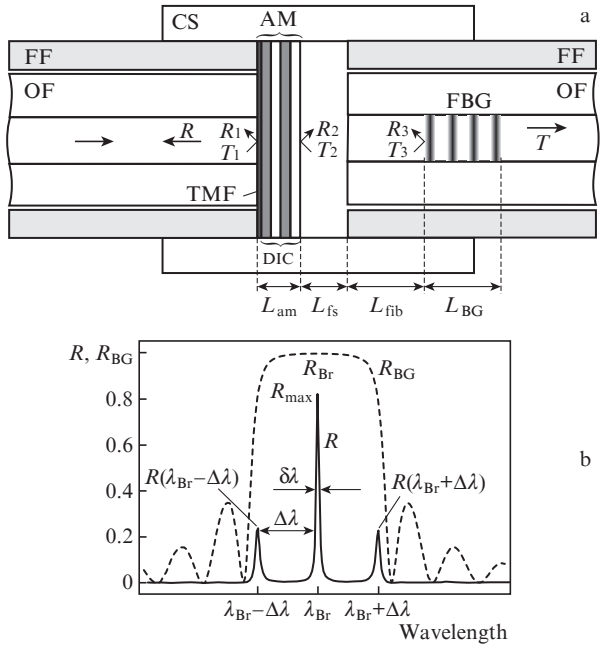

Figure 1. Narrow-band reflection filter: (a) schematic of the cavity and (b) reflection spectra of the filter (R) and FBG (R_{BG}):
(OF) single-mode optical fibre; (FF) fibre ferrule; (CS) cylindrical spring; (TMF) thin metallic film; (DIC) dielectric interference coating; (AM) asymmetric mirror; $R_{1,2,3}$ and $T_{1,3}$ are the reflectances and transmittances of the mirrors; L_{am}, L_{fs}, L_{fib} and L_{BG} are the lengths of the corresponding sections; R_{max} is the maximum reflectance; $\delta\lambda$ is the full width at half maximum; $\Delta\lambda$ is the free spectral range of the filter; and R_{Br} is the reflectance of the FBG at the Bragg wavelength λ_{Br}.

It is seen from (1) that reflectance R is determined by interference of two beams: the 'zero' beam (of amplitude r_1), reflected from the AM, and the beam that emerges from the cavity and is the result of multiple-beam interference. Transmittance T in (2) is determined by the transmitted beam only. In the case of two-beam reflection interference, the shape of the reflection spectrum will change and the picture will become asymmetric if the phases of the amplitude coefficients of the AM will be varied, which is possible for lossy mirrors. For example, a phase combination $\theta = \Psi_1 + \Psi_2 - 2\Phi_1 \neq m\pi$ (where m is an integer) will produce asymmetric reflection peaks [9, 13], whereas totally symmetric peaks result at $\theta = m\pi$ or in the case $R_1 = 0$ [for a lossless mirror at $\theta = (2m + 1)\pi$].

Parameters of the asymmetric mirror are rather difficult to calculate in detail, because parameters of both the film and matched dielectric coating should be taken into account, but parameters of the interferometer with the AM under consideration, having power coefficients $R_1 = 0$ and $T_1 = (1 - R_2)/2$, can be described with rather high accuracy. Relation (1) will then be equivalent to (2) to within a constant factor [14]. In this case, $\psi = (\Psi_2 + \Psi_3)/2 - \pi m$ corresponds to the maximum reflectance:

$$R_{max} = \frac{(1 - R_2)^2 R_3}{4(1 - \sqrt{R_2 R_3})^2}. \quad (3)$$

It follows from (3) that, at $R_3 = 1$, we have $R_{max} = (1 + \sqrt{R_2})^2/4$. In practice, the condition $R_1 = 0$ is rather difficult to meet, so in real interferometers there is always a contribution of the zero beam to the asymmetry of the spectrum [9]. For $R_1 \to 0$, the interference fringe finesse is

$$F = \frac{\pi \sqrt[4]{R_2 R_3}}{1 - \sqrt{R_2 R_3}}. \quad (4)$$

At a given scatter in the refractive index of the core, the length of the cavity back mirror (FBG), L_{BG}, influences the width of the reflection spectrum, reflectance $R_{BG}(\lambda)$ and maximum reflectance $R_{Br} = R_{BG}(\lambda_{Br})$ at the Bragg wavelength λ_{Br} (Fig. 1b). Substituting $R_3 = R_{BG}$ into (1) and phase-matching the air gap length L_{fs}, we can obtain one strong, central peak R_{max} at the wavelength λ_{Br} and two weaker, side peaks at wavelengths $\lambda_{Br} \pm \Delta\lambda$ (Fig. 1b). The degree of light filtering (full spectral width at half maximum), $\delta\lambda$, can be evaluated from the fringe finesse F and the admissible free spectral range $\Delta\lambda$ [i.e. the optical length of the interferometer base, $L \approx \lambda_{Br}^2/(2\Delta\lambda)$, at which the side peaks are much weaker than the central peak]:

$$\delta\lambda = \Delta\lambda/F. \quad (5)$$

Thus, to raise the degree of filtering, one should maximise the interference fringe finesse F (to the realistic level $F = 10^2 - 10^3$) and the reflectance of the FBG ($R_{Br} \to 1$) and minimise $\Delta\lambda$. The last parameter is determined by the spectral width of the FBG and the shape of its spectrum, as well as by the conditions under which the filter is employed, i.e. by the constraints on the admissible relationship between the heights of the central and neighbouring peaks: $R(\lambda_{Br} \pm \Delta\lambda)/R_{max} \ll 1$. The cavity Q-factor in the interferometer under consideration is essentially equivalent to its resolving power: $Q = \omega_0/\delta\omega \approx \lambda_0/\delta\lambda$, $\delta\lambda \ll \lambda_0$ (λ_0 is the peak reflection wavelength).

Relations (3) and (4) do not explicitly take into account the transmission loss during light propagation in the interferometer base. Nevertheless, this loss can be included in R_2 and/or R_3. Figure 2 shows contour plots of the maximum reflectance [Eqn (3)] and fringe finesse [Eqn (4)] as functions of R_2 and R_3. R_{max} reaches the highest level only in the case of an optically dense back mirror ($R_3 \to 1$). It is then important that the condition $R_2 < R_3$ be fulfilled, otherwise R_{max} decreases, as follows from (3). In practice, realistic values are $R_2 = 0.95$ and $R_3 = 0.988$, which give $R_{max} \approx 0.65$ and $F \approx 100$ (point I). It is seen in Fig. 2 that, to obtain $R(\lambda_{Br} \pm \Delta\lambda)/R_{max} < 10^{-1}$, we should have $R_3 < 0.85$ (point II). At $R_3 = 0.5$, the above ratio is under 10^{-2}. If $\Delta\lambda$ is the full width at half maximum (FWHM) of the reflection spectrum of the FBG, $\delta\lambda$ will be two orders of magnitude smaller than the spectral width of the FBG.

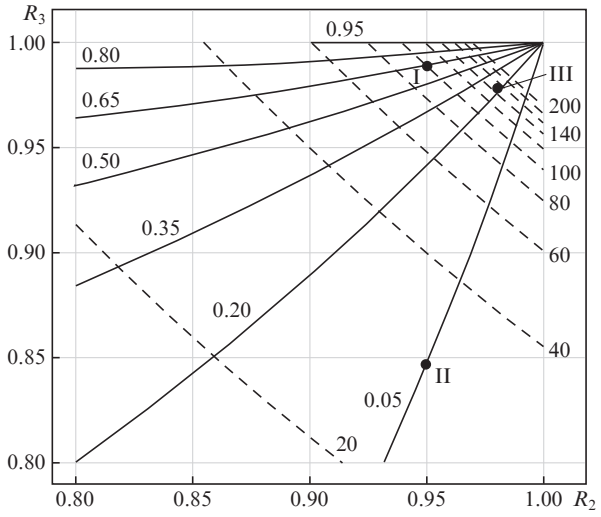

Figure 2. Contour plots of the maximum reflectance R_{max} (solid lines) and fringe finesse F (dashed lines) of the filter as functions of R_2 and R_3: (I, II) calculation results, (III) experimental data point.

3. Fabrication of the constituent parts of the interferometer

The asymmetric mirror was fabricated as described previously [8, 9]. A key component of the AM was a polished end facet of SMF-28e glued into a fibre ferrule. A thin metallic nickel film was produced on the facet by vacuum magnetron sputtering in an argon atmosphere (10^{-3} mm Hg). Next, TiO_2 and SiO_2 layers were sequentially grown by the same technique in a mixture of argon (2.5×10^{-3} mm Hg) and oxygen (10^{-3} mm Hg) using a titanium and a silicon target, respectively. The parameters of the film are of critical importance and should meet the matching condition $n = (1 - R_{Ni} - T_{Ni})/T_{Ni}$, where R_{Ni} and T_{Ni} are the reflectance and transmittance of the nickel film on the fibre side ($R_{Ni} \approx 0.14$). The deposition of the dielectrics on the film was monitored by following the time variation of reflectance R_1 at a wavelength of 1550 nm during the growth of the dielectric film. The first layer was from TiO_2 and a change in dielectric material corresponded to an extremum in R_1 [9, 10]. Interference of the light reflected from the film and dielectric coating led to an increase in Ohmic loss in the film. Thus, R_1 can be gradually reduced down to zero (or to a negligible level) and the reflectance on the opposite side of the mirror, R_2, can be brought to near unity via optical densification of the multilayer dielectric coating. Nine dielectric layers were produced on the film, which ensured $R_1 \approx 2 \times 10^{-3}$.

The back mirror (FBG) was produced in the core of the same OF. Figure 3a shows a schematic of the experimental setup used for FBG inscription. During the grating inscription process, a motorised linear translation stage, with a phase mask and optical fibre secured to it, moved across a UV laser beam ($\lambda \approx 244$ nm) (see e. g. Ref. [15]). The laser beam, with a Gaussian intensity profile (beam diameter of 1.2 mm), was focused by cylindrical lens into the fibre core. The grating had a uniform refractive index profile almost throughout its length because the fibre was translated steadily across the overlap (interference) region of the diffracting beams except in the peripheral part, where there was a 0.6-mm-long transition region.

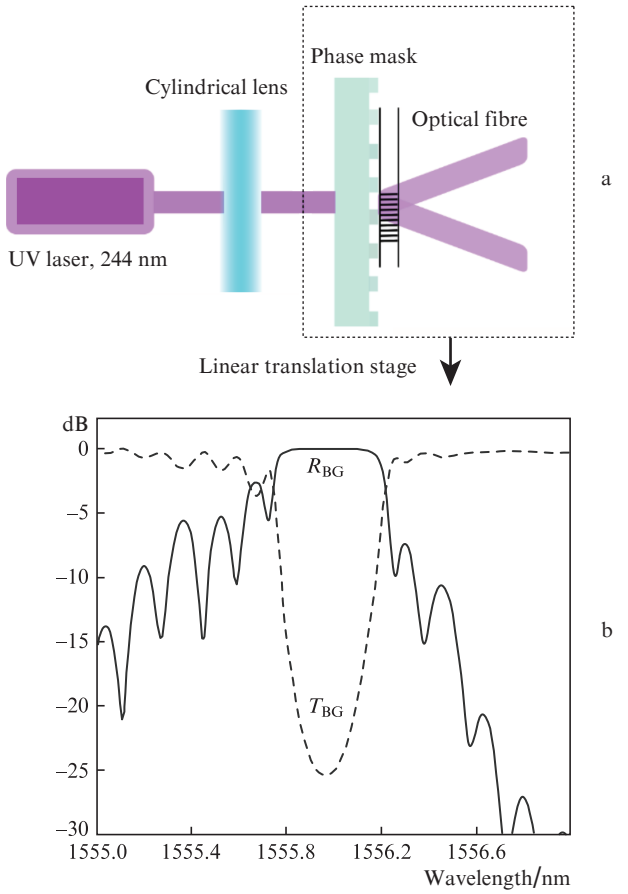

Figure 3. FBG formation: (a) schematic of the writing process and (b) reflection (R_{BG}) and transmission (T_{BG}) spectra of the FBG.

To produce a cavity base, the fibre was cleaved 1.5 cm away from the FBG edge and thermally glued into a fibre ferrule with Canada balsam. Next, the end face of the ferrule was polished across the fibre axis (the final polishing film had a grain size of 0.02 μm). The reflection and transmission spectra of the FBG changed insignificantly in comparison with those taken before the fibre was glued into the ferrule. Canada balsam was applied only to the L_{fib} section of the fibre to avoid distortion of the spectrum as a result of possible fibre deformation by solidified balsam particles. Figure 3b shows the reflection and transmission spectra of the FBG measured with a

Yokogawa AQ6370 optical spectrum analyser. The centre wavelength of the grating was 1555.7 nm (spectral resolution of 20 pm). The 3 dB (half-maximum) bandwidth of the spectrum was 235 pm (260 pm between the first minima), and the dip in the transmission spectrum was −25.5 dB (2.8×10^{-3}). The parameters of the FBG were calculated in the uniform grating approximation using formulas presented elsewhere [12, 16]: $L_{\text{eff}} = 1.33$ mm at $L_{\text{BG}} = 9.7$ mm.

4. Measurement system

Figure 4 shows a schematic of the experimental setup used to measure characteristics of the interferometer. The light source used was a superluminescent diode (SLD) with a centre wavelength of 1530 nm, full spectral width at half maximum of 45 nm and output power of 20 mW. After the SLD was placed an optical isolator (OI). The fibre circulator (FC) directed light from the input port to the medium one. To prevent degradation of the asymmetric mirror by high light intensity, we used a mechanically tunable Fabry–Perot filter with a spectral width of 1 nm, which was tuned to the centre wavelength of the FBG. After the filter were placed an FC/PC fibre butt joint (FBJ) and then the reflection interferometer (AM and FBG). The total optical power incident on the AM was measured after the TF with the FBJ disconnected and was 120 μW. The reflected light was directed by the circulator to the output port through a polarisation controller (PC) and to an Apex 2050A optical spectrum analyser (resolving power, 0.04 pm).

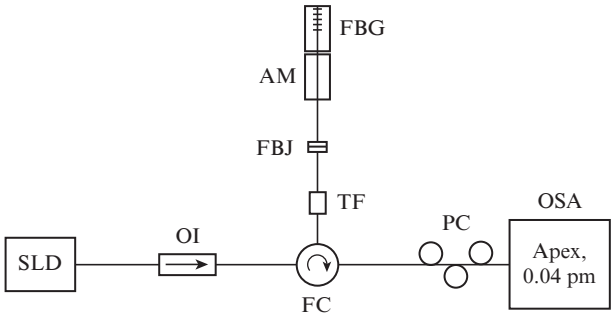

Figure 4. Schematic of the measurement setup: (SLD) superluminescent diode; (OI) optical isolator; (FC) fibre circulator; (TF) tunable filter; (FBJ) FC/PC fibre butt joint; (AM) asymmetric mirror; (PC) polarisation controller; (OSA) Apex AP2050A optical spectrum analyser.

5. Experimental results

Figure 5a shows the reflection spectrum of the FBG (R_{BG}) in a narrow spectral range (±200 pm) relative to the height of one of the reflection peaks of the interferometer, R.

The spectrum of the FBG was measured with the FBG and FBJ ferrules joined. It seems likely that, as a result, the FBG was deformed because of the fibre bend and its spectrum shifted to longer wavelengths by several tens of picometres. This accounts for the discrepancy between the positions of the reflection peaks of the interferometer and FBG. The maximum reflectance of the interferometer, R_{max}, was determined as the ratio of the maximum intensity of peak P_0 to the reflectance R_{BG} of the FBG at the peak reflection wavelength and was thus found to be 0.21 (−6.8 dB) (a similar result will be obtained if R_{max} will be determined relative to the average background level, which should be at a level $R_1 \approx 2\times10^{-3}$).

The reflection spectrum of the interferometer, R, contains four distinct peaks: P_{-2},P_{-1}, P_0 and P_1. The two strong, central peaks (P_{-1} and P_0) have roughly equal heights. The spectral separation between them is $\Delta\lambda = 76.2$ pm, which corresponds to $L_{\text{fs}} \approx 5$ μm and $L_{\text{fib}} \approx 9.4$ mm (at $L_{\text{eff}} = 1.33$ mm). Peak P_0 is shown in greater detail in Fig. 5b. Its 3 dB width $\delta\lambda$ is 0.5 pm (~62 MHz, $Q \approx 3\times10^6$), which corresponds to $F \approx 150$ (Fig. 2, point III). The other strong peak, P_{-1}, has an FWHM near 0.6 pm. The parameters of the interferometer under consideration are of the same order as those of a narrow-band reflector based on a whispering gallery mode ring cavity [17], in which reflection is due to scattering by inhomogeneities of the cavity wall [18]. Both peaks have asymmetric profiles. Moreover, the strong peaks P_{-1} and P_0 have two nearby polarisation side peaks (PP_{-1} and PP_0), which can be suppressed using a polarisation controller (it seems likely that they originate from the inherent polarisation dependence of the optical spectrum analyser rather than from the birefringence in the structure of the interferometer). Another two side peaks (P_{-2} and P_1) have a much lower intensity and larger spectral width, which is attributable to the decrease in R_{BG} at the edges of the reflection band. Because of the low intensity, the spectra presented in Fig. 5 are very noisy, so we performed Gaussian smoothing ($\sigma = 5$) of the raw data. As seen in Fig. 5, the interferometer finesse, i.e. the ratio of the maximum to minimum reflectance, is about 20 dB (it may be that it is limited by the sensitivity of the OSA). The difference in peak intensity between P_0 and P_{-2} is about 13 dB.

Reducing the length of the fibre section in the base, L_{fib}, can ensure that only one peak remains within the reflection band of the FBG. It is then reasonable to expect its width to increase to ~1 pm. At the same time, if we reduce the width

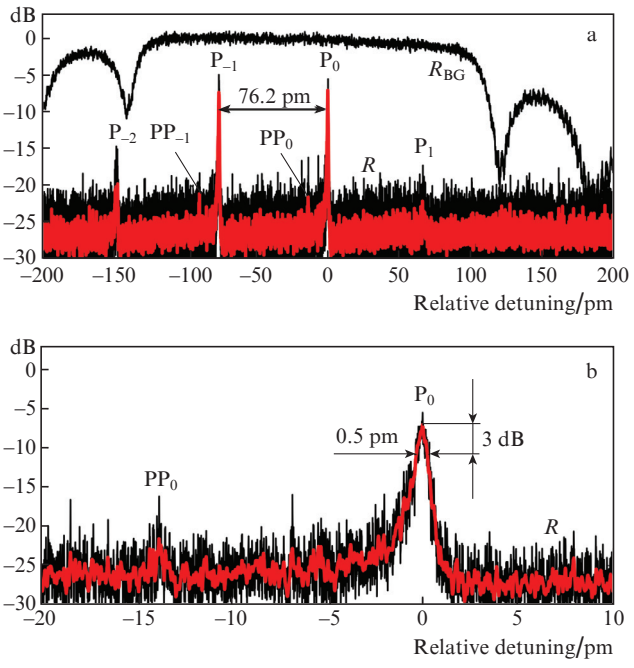

Figure 5. (a) Reflection spectra of the reflection interferometer and (b) peak P_0 ($\lambda = 1556.116$ nm) in a narrow wavelength range. The grey line represents Gaussian smoothing results, P_i are the reflection peaks of the filter, and PP_i are polarisation peaks ($i = -2, -1, 0, 1$).

of the reflection spectrum of the FBG to 50 pm, while maintaining R_{BG} near unity, which is quite possible in the case of UV FBG inscription, the interferometer base length and degree of filtering can be increased. The cavity Q-factor can also be raised: by increasing the reflectances of the mirrors. According to our estimates, the described approach enables filtering at a level of 0.1 pm (12 MHz at $\lambda = 1550$ nm) due to a reduction in the spectral width of the FBG by a factor of 3–4 and an increase in fringe finesse by a factor of 2–3. It is worth noting that, in the proposed approach, the selection wavelength can readily be changed by replacing the right-hand ferrule, which encloses the FBG (Fig. 1a), by another one to ensure filtering at a preset wavelength (within the operating range of the AM). Using a piezoceramic transducer, the length L_{fs} can be fine-tuned so as to gradually vary the peak reflection wavelength of the interferometer within its free spectral range.

The described method is applicable throughout the spectral range where the constituent components of the interferometer are capable of operating, and it can be combined with other types of single-mode fibre, e. g. with birefringent one (of the PANDA type). Given the good optical damage resistance of the fibre material, this type of filter can be used for selecting laser modes and obtaining up to 10 mW of output power in single-mode fibre at a wavelength of 1550 nm. As shown earlier [19], if a diffraction structure is used instead of the thin metallic film on the mirror, the optical damage threshold of the interferometer can be maximised, enabling it to operate at powers above 100 mW.

6. Conclusions

We have described a method for reflection filtering of light using a fibre reflection interferometer based on an asymmetric reflectance front mirror and a fibre Bragg grating as a back mirror. Formulas have been presented for calculating parameters of the interferometer (fringe finesse and maximum reflectance). We have described the fabrication of a test sample and measurements of its characteristics. The spectral width of its reflection band is 0.5 pm (62 MHz, $Q \approx 3 \times 10^6$) at a wavelength of 1556 nm, its maximum reflectance is 0.21, and its contrast is 10^2. The present results suggest that the proposed method can be used to fabricate narrow-band reflection fibre filters with a degree of selection up to 0.1 pm at a wavelength of 1550 nm.

Acknowledgements. This work was supported by the Russian Science Foundation (Project No. 14-22-00118). In our experimental work, we used equipment at the Spectroscopy and Optics Shared Research Facilities Centre, Institute of Automation and Electrometry, Siberian Branch, Russian Academy of Sciences, and at the Fiber Lasers Laboratory, Department of Physics, Novosibirsk State University.

We are grateful to I.D. Vatnik for his assistance in the experimental work.

References

1. Gallegos-Arellano E., Vargas-Rodriguez E., Guzman-Chavez A.D., Cano-Contreras M., Cruz J.L., Raja-Ibrahim R.K. *Laser Phys. Lett.*, **13**, 065102 (2016).
2. DiLazaro T., Nehmetallah G. *Opt. Express*, **26**, 2891 (2018).
3. Scheuer J., Sumetsky M. *Laser Photonics Rev.*, **5** (4), 465 (2011).
4. Collodo M., Sedlmeir F., Sprenger B., Svitlov S., Wang L., Schwefel H. *Opt. Express*, **22**, 19277 (2014).
5. Kawasaki B.S., Hill K.O., Johnson D.C., Fujii Y. *Opt. Lett.*, **3**, 66 (1978).
6. Dostovalov A.V., Wolf A.A., Parygin A.V., Zyubin V.E., Babin S.A. *Opt. Express*, **24**, 16232 (2016).
7. Chung Y., Kim D., Dagli N. *J. Lightwave Technol.*, **24**, 1865 (2006).
8. Terentyev V.S., Simonov V.A., Babin S.A. *Laser Phys. Lett.*, **14**, 25103 (2017).
9. Terentyev V.S., Simonov V.A., Babin S.A. *Opt. Express*, **24**, 4512 (2016).
10. Kamenev N.N., Troitskii Yu.V. *Opt. Spektrosk.*, **54**, 725 (1983).
11. Troitskii Yu.V. *Mnogoluchevye interferometry otrazhennogo sveta* (Multiple Beam Reflected-Light Interferometers) (Novosibirsk: Nauka, 1985).
12. Barmenkov Y.O., Zalvidea D., Torres-Peiró S., Cruz J.L., Andrés M.V. *Opt. Express*, **14**, 6394 (2006).
13. Chen L., Han Y., Liu Q., Liu Y.-G., Zhang W., Chou K.C. *Opt. Lett.*, **43**, 1662 (2018).
14. Kol'chenko A.P., Terent'ev V.S., Troshin B.I. *Opt. Spectrosc.*, **101** (4), 632 (2006).
15. Abdullina S.R., Nemov I.N., Babin S.A. *Quantum Electron.*, **42**, 794 (2012) [*Kvantovaya Elektron.*, **42**, 794 (2012)].
16. Vasil'ev S.A., Medvedkov O.I., Korolev I.G., Bozhkov A.S., Kurkov A.S., Dianov E.M. *Quantum Electron.*, **35**, 1085 (2005) [*Kvantovaya Elektron.*, **35**, 1085 (2005)].
17. Rivera-Pérez E., Díez A., Andrés M.V., Cruz J.L., Rodríguez-Cobos A. *Opt. Lett.*, **38**, 1636 (2013).
18. Gorodetsky M.L., Pryamikov A.D., Ilchenko V.S. *J. Opt. Soc. Am. B*, **17**, 1051 (2000).
19. Terentyev V.S., Simonov V.A. *Quantum Electron.*, **47**, 971 (2017) [*Kvantovaya Elektron.*, **47**, 971 (2017)].